Geophysical Research Letters

RESEARCH LETTER
10.1029/2018GL077309

Special Section:
The Arctic: An AGU Joint Special Collection

# Variations in Gas and Water Pulses at an Arctic Seep: Fluid Sources and Methane Transport

W.-L. Hong[1,2], M. E. Torres[3], A. Portnov[2,4], M. Waage[2], B. Haley[3], and A. Lepland[1]

[1]Geological Survey of Norway, Trondheim, Norway, [2]Centre for Arctic Gas Hydrate, Environment and Climate, Arctic University of Norway (UiT), Tromsø, Norway, [3]College of Earth, Ocean, and Atmospheric Sciences, Oregon State University, Corvallis, OR, USA, [4]School of Earth Sciences, Ohio State University, Columbus, OH, USA

**Key Points:**
- We document the decoupled gaseous and aqueous fluid phases from Storfjordrenna, a cold seep south of Svalbard
- We propose a three-stage evolution model with different modes of methane transport in each stage
- The evolution of the seepage is controlled by the availability of gaseous methane and/or the development of fluid conduits

**Supporting Information:**
- Supporting Information S1
- Data Set S1

**Correspondence to:**
W.-L. Hong,
wei-li.hong@ngu.no

**Citation:**
Hong, W.-L., Torres, M. E., Portnov, A., Waage, M., Haley, B., & Lepland, A. (2018). Variations in gas and water pulses at an Arctic seep: Fluid sources and methane transport. *Geophysical Research Letters*, *45*. https://doi.org/10.1029/2018GL077309

Received 27 JAN 2018
Accepted 4 APR 2018
Accepted article online 19 APR 2018



**Abstract** Methane fluxes into the oceans are largely dependent on the methane phase as it migrates upward through the sediments. Here we document decoupled methane transport by gaseous and aqueous phases in Storfjordrenna (offshore Svalbard) and propose a three-stage evolution model for active seepage in the region where gas hydrates are present in the shallow subsurface. In a preactive seepage stage, solute diffusion is the primary transport mechanism for methane in the dissolved phase. Fluids containing dissolved methane have high $^{87}Sr/^{86}Sr$ ratios due to silicate weathering in the microbial methanogenesis zone. During the active seepage stage, migration of gaseous methane results in near-seafloor gas hydrate formation and vigorous seafloor gas discharge with a thermogenic fingerprint. In the postactive seepage stage, the high concentration of dissolved lithium points to the contribution of a deeper-sourced aqueous fluid, which we postulate advects upward following cessation of gas discharge.

**Plain Language Summary** How methane moves in the marine sediment, as a gas or a dissolved component, determines the environmental impact of this important greenhouse gas. In contrast to observations of biosphere activity beeing supported by dissolved methane, free gas methane cannot be used by microorganisms and can escape to the ocean more easily. Here we report the different ways methane moves in the sediments of an Arctic methane seep. We show that methane moves as free gas during the most active stage and as a dissolved component in the pore water before and after the most active period. Our results show that the supply of free gas methane in the sediments can explain why some of the seafloor features in our study area are more active than the others.

## 1. Introduction

Continental margin sediments constitute the largest known natural hydrocarbon source to the global ocean (Hovland et al., 1993; Kvenvolden & Rogers, 2005; Reeburgh, 2007). Methane emission at the seafloor necessitates transport through the sediment either in the gas phase or as a dissolved constituent in pore water. Dissolved methane migrates by diffusion and/or it can be transported with the aqueous phase (i.e., advection). Most of the dissolved methane is consumed by microorganisms within the upper few meters of sediments through aerobic and anaerobic oxidation of methane (AeOM and AOM, respectively; Boetius & Wenzhofer, 2013), which limit methane escape to the overlying water column (Chen et al., 2017; Regnier et al., 2011). Microorganisms cannot utilize methane in the gas phase; therefore, in areas of intense upward fluid migration, where the methane concentration exceeds solubility, methane gas bypasses the microbial filter and escapes into the water column. Methane bubbling into the water column from the seafloor has been widely documented through direct observations (Haeckel et al., 2004; MacDonald et al., 1994; McVeigh et al., 2018; Sahling et al., 2014; Sauter et al., 2006) as well as by hydrocasts and hydroacoustic surveys (Greinert et al., 2010; Greinert et al., 2013; Mau et al., 2017; Nikolovska et al., 2008; Römer et al., 2012; Smith et al., 2014).

Here we report on pore water geochemistry and geophysical observations from a recently described field of gas hydrate mounds (GHMs) in the Storfjordrenna Trough Mouth Fan, south of Svalbard (Figures 1a and 1b). Persistent hydroacoustic anomalies were detected in the water column above four of the surveyed GHMs (Serov et al., 2017) and abundant gas hydrates were recovered in the sediments of these features by gravity coring (Hong et al., 2017). GHM5 is the exception as from this mound there are neither hydroacoustic anomalies nor gas hydrates, despite its close proximity ($<$1 km) to other GHMs. We mapped the distribution of gas-related amplitude anomalies in 3-D seismic data and inferred the origin of methane gas from its stable

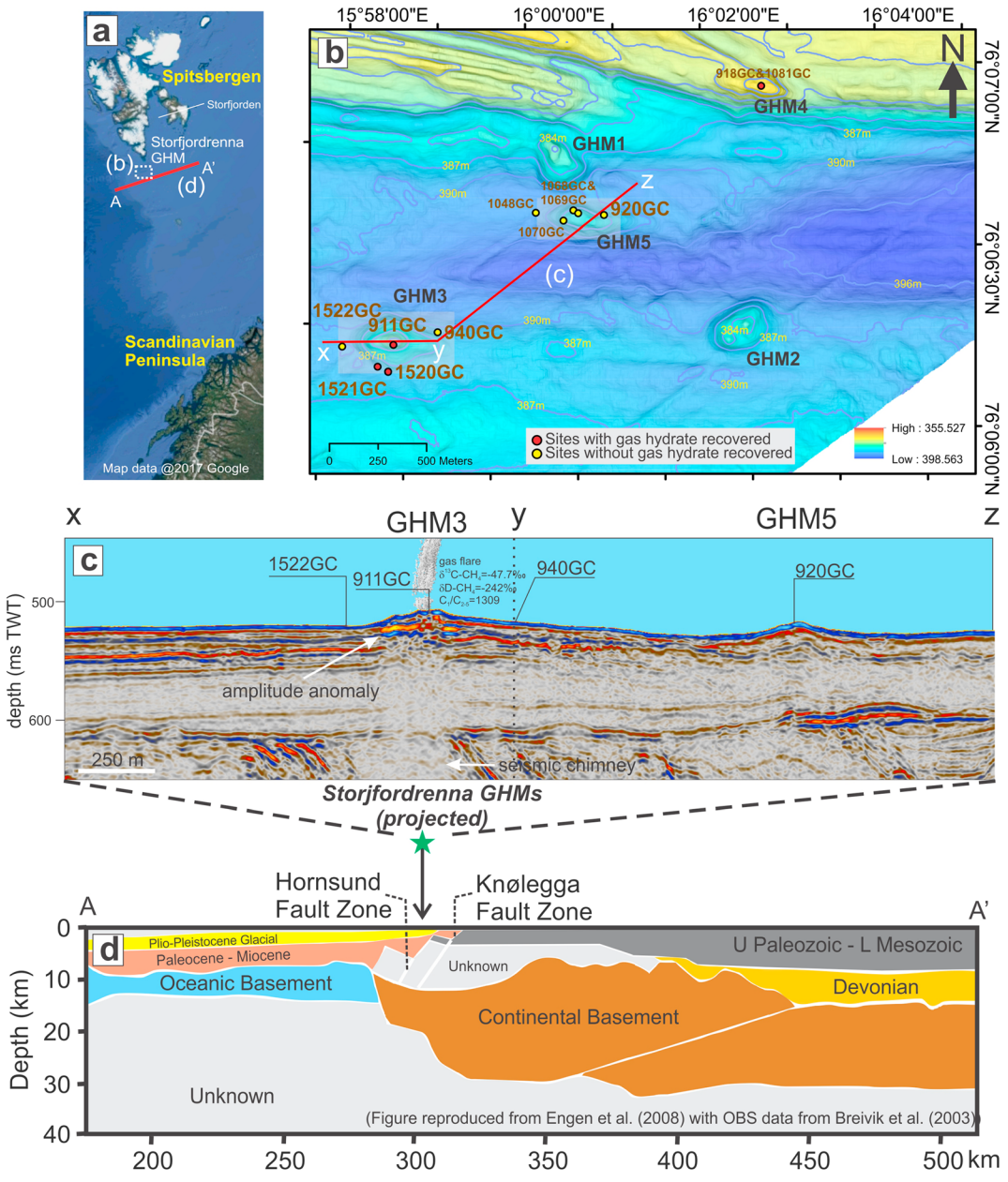


**Figure 1.** (a) A regional map showing the study area and the location of the deep seismic profile in panel d. (b) Detailed bathymetry map showing the investigated sediment cores. We focused on the completed data set from the six sites (larger label fonts in b) and showed available data for the other six sites (smaller label fonts in b) in the supporting information. The red line (*x*-*y*-*z*) marks the location of the *P* cable seismic line in panel c across the two investigated gas hydrate mounds (GHMs) with the stable isotopic signatures of a gas bubble sample collected. (d) Structural geological profile (modified after Engen et al., 2008) showing the location of the two major fault systems in relation to Storfjordrenna GHMs.

isotopic signatures. These data were combined with results of pore water geochemistry analyses to infer sources of the aqueous phase and water-rock interactions. Based on these results, we hypothesize that the observed contrasting seepage activities reflects the different evolutionary stages of the system, controlled by the transport of different fluid phases (i.e., gas versus water). Our observations provide critical constraints for the fluid migration within this shallow water Arctic gas hydrate field, which serves as an example for other cold seeps along continental margins worldwide.

## 2. Geological Setting and Site Description

The Storfjordrenna GHMs are located ~50 km south of Spitsbergen at ~390 m water depth (Figure 1b). Two major fault systems cut across this region: the Hornsund Fault Zone (HFZ; also known as De Geer Fracture Zone) and the Knølegga Fault Complex (KFC) (Figure 1d). The HFZ is located at the western edge of the continental basement, adjacent to the continent-ocean boundary (Breivik et al., 2003). To the east of HFZ, the subparallel development of the KFC represents the down-faulted terrace of the continental crust, which is considered as a part of the Hornsund fault complex (Gabrielsen, 1984; Myhre et al., 1982; Sundvor & Eldholm, 1976). The HFZ was proposed to serve as a pathway for methane transport, based on multiple gas seepage sites observed from 72° to 79°N that coincide with this structural lineament (Mau et al., 2017).

Glacial cycles in this region have strongly modulated sediment transport, seafloor topography, and the subseafloor pressure regime (Ingólfsson & Landvik, 2013; Patton et al., 2016; Wegner et al., 2015). Repeated glaciations led to alternation of depositional and erosional processes which, in the Storfjordrenna region, is reflected in a ~50–150-m-thick upper glacial unit (Elverhøi & Solheim, 1983). In addition, isostatic adjustment associated with deglaciation (Patton et al., 2016) has been shown to play an important role in the reactivation of faults and the seismicity of the region, which also in turn facilitates fluid migration (Mörner, 1978; Stewart et al., 2000) and may potentially destabilizes gas hydrate in the sediments (Wallmann et al., 2018).

In our study area, the glacial/glacial-marine clays and silts are mainly composed of quartz (20%–40%), feldspar (5%–15%), carbonates (10%–20%) and clay minerals (Andersen et al., 1996). As documented in Hong et al. (2017), cores recovered from the GHMs contain abundant methane-derived authigenic carbonate nodules. At sites with active gas discharge, gas hydrates occurred as shallow as 0.85 meters below seafloor (mbsf). Datings of two planktonic foraminifera specimens from a 3.2-m-long gravity core without any sign of active methane discharge (1522GC in Figure 1b) yield an age for the bottom of this core slightly older than 16.2 kyr BP whereas the upper 70 cm is of Holocene age (Hong et al., 2017).

## 3. Methods

Sampling and analytical methods for pore water and gas samples are detailed in the supporting information with data included in Data Set S1. The seismic data used in this study were obtained during a 3-D seismic P-Cable survey in 2016, which generated a broadband high-resolution data set (~6 m horizontal and ~3 m vertical) suitable for mapping geological structures in the shallow subsurface ($<$1,000 mbsf). Details of data acquisition and processing were given in Petersen et al. (2010).

## 4. Results and Discussion

Pore water data from the six investigated sites were presented in Figure 2 (See Table S1 of the supporting information for site location and water depths). We included the available data from six additional sites (labeled with smaller fonts in Figure 1b) in the supporting information to generalize our observations. However, as the data set is not as complete in these six additional sites as in the others, we do not focus our discussion on them. In general, sulfate concentrations decrease with depth either in a monotonic (1522GC and 920GC) or in a nonlinear fashion (911GC, 940GC, 1520GC, and 1521GC). After considering various processes that can lead to nonsteady state pore water profiles, Hong et al. (2017) concluded that such pore water profiles result from a recent increase in methane flux. Also, aqueous advection is insignificant at the active sites despite the shallow ($<$1 mbsf) sulfate–methane-transition-zone (SMTZ). Rather, diffusion of methane from a shallow fluid flow system, as seen from the seismic profile (Figure 1c), sustains the high AOM rates observed from these sites.

Chloride concentrations are close to the seawater value (558 mM) at most sites, with downcore increasing and decreasing trends observed in 920GC and 1522GC, respectively (Figure 2). It is well-established that gas hydrate dissociation during core recovery can dilute the concentrations of all ions including chloride while rapid gas hydrate formation can result in chloride content higher than the seawater value (Haeckel et al., 2004; Torres et al., 2004, 2011; Ussler & Paull, 2001). However, there is no sufficient methane flux to sustain gas hydrate formation at 920GC and 1522GC (Serov et al., 2017) and, consequently, no gas hydrate was recovered from either site (Hong et al., 2017). Therefore, we are confident that the observed chloride variations at 920GC and 1522GC are not related to gas hydrate dissociation and/or formation. Other potential freshening sources include dehydration of clay minerals at depth (Kastner et al., 1991; Kim et al., 2013),

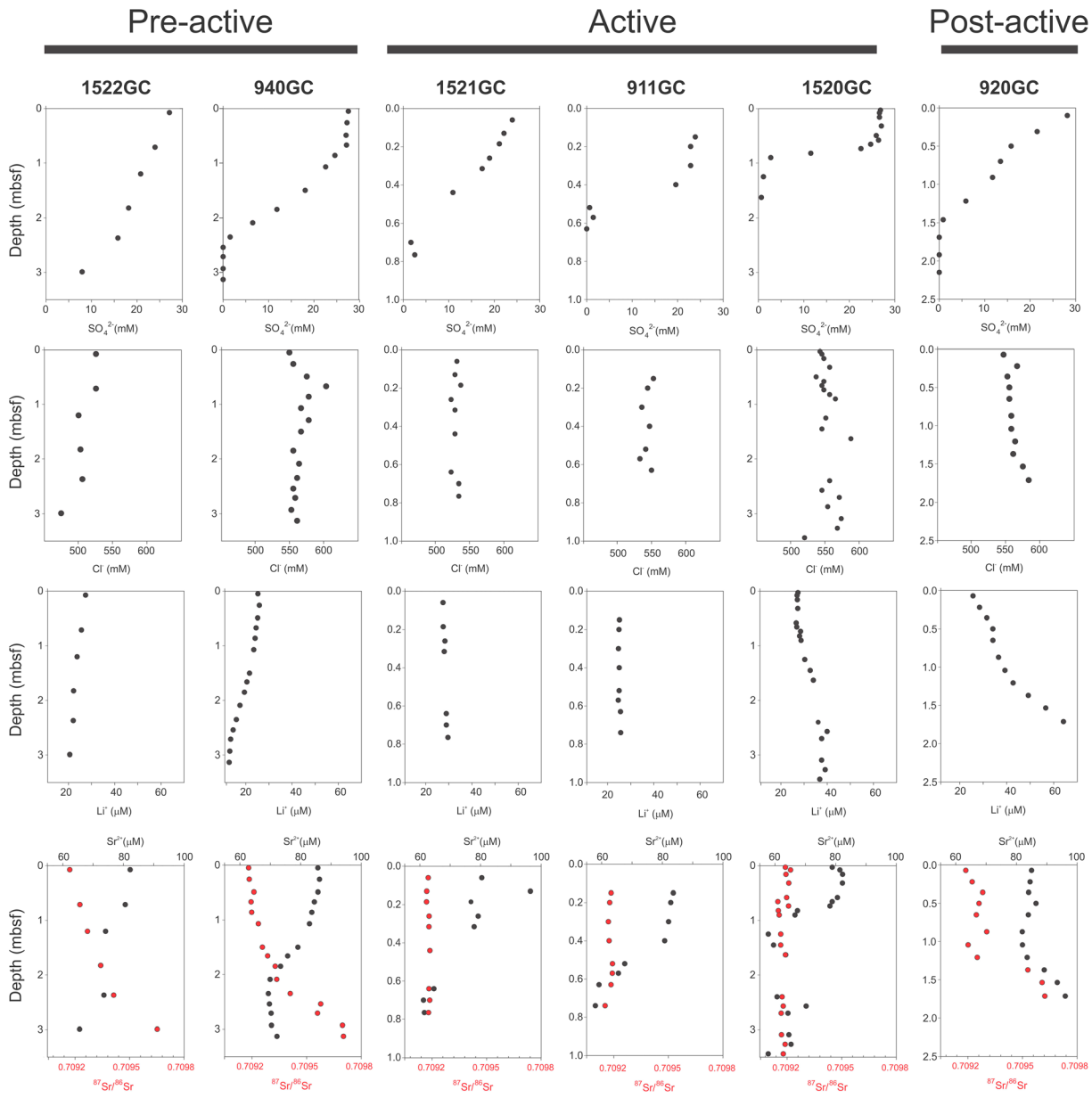


**Figure 2.** Pore water data from the six investigated sites. The sites were arranged based on the proposed evolution of the seepage (see text for more details). Note that the depth scales are different at the different sites.

clay membrane ion filtration (Haydon & Graf, 1986), and/or mixing of a meteoric water source (Post et al., 2013). Potential fluid sources with chloride content higher than seawater include the residual water from clay membrane ion filtration, formation of clay minerals, and/or contribution from a brine (Kastner et al., 1991). Brine production in Storfjorden (Figure 1a) has been documented from ocean conductivity, temperature, and pressure data (Skogseth et al., 2005) and the ratio of agglutinated and calcareous foraminifera in the sediment records (Rasmussen & Thomsen, 2014). Such brine might explain the elevated chloride concentration. However, the exact causes of the variations in chloride concentration observed in cores 1522GC and 920GC are not clear at present and await further investigation. For the three sites where gas hydrates were recovered (911GC, 1520GC, and 1521GC), chloride concentrations are scattered around the seawater value, likely reflecting gas hydrate formation/dissociation.

We observed large variations in lithium and strontium concentrations as well as strontium isotopic ratios across the investigated sites. The lithium concentration decreases with depth at the two sites with the

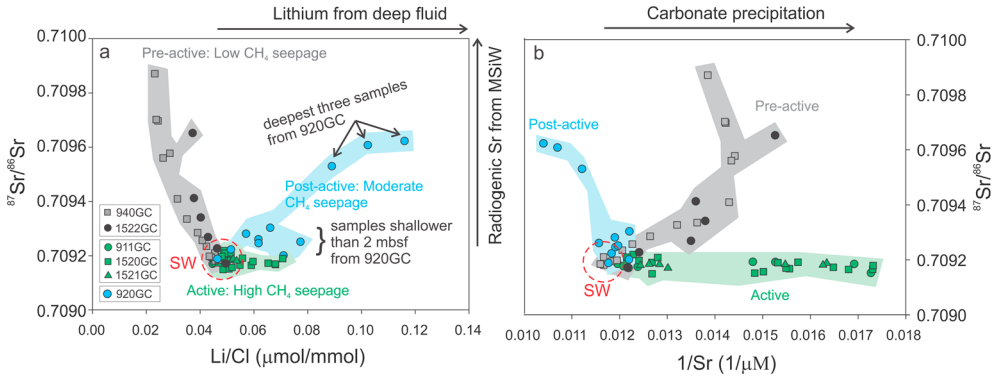


**Figure 3.** Cross-plot of (a) Sr isotopic ratios versus Li/Cl ratios and (b) Sr isotopic ratios versus 1/Sr. See text for explanation of each end members. MSiW = marine silicate weathering.

deepest SMTZ (1522GC and 940GC; Figure 2), whereas the concentration stays close to a seawater value at the sites with the shallowest SMTZ (911GC, 1520GC, and 1521GC; Figure 2). Pore water lithium concentrations increase up to double seawater value at 920GC (Figure 2), where the SMTZ is at intermediate depth. Strontium concentrations at most of the sites decrease from the seawater value to a minimum at the depth of SMTZ due to the intensive precipitation of authigenic carbonates (Hong et al., 2017) and remain below the seawater concentration throughout the rest of cores (Figure 2). Only at 920GC, strontium concentrations significantly increase in the deepest three samples. The $^{87}Sr/^{86}Sr$ ratio increases from a seawater value of 0.709217 downcore at the three sites with deeper SMTZ (1522GC, 940GC, and 920GC), whereas the ratios are slightly lower than seawater value throughout the cores at the sites with shallow SMTZ (911GC, 1520GC, and 1521GC).

### 4.1. Multiple Fluid Sources Inferred From Pore Water Geochemistry

We observed distinct grouping of values among the investigated sites when we compared the $^{87}Sr/^{86}Sr$ ratios against Li/Cl in Figure 3a and against the inverse of strontium concentrations in Figure 3b. At sites with low methane flux (gray area in Figure 3), the strontium concentrations lower than the seawater value (88 μM) are due to intense carbonate precipitation whereas the high $^{87}Sr/^{86}Sr$ ratios in the pore water (up to 0.7099 and 0.7098 at 1522GC and 940GC, respectively; Figure 3a) are indicative of ongoing weathering of silicate minerals in marine sediments (i.e., marine silicate weathering or MSiW hereafter). It has been shown that MSiW occurs in the microbial methanogenesis zone due to the lowering of pH associated with fermentation and resulting $CO_2$ production (Kim et al., 2016; Solomon et al., 2014; Wallmann et al., 2008). The release of strontium due to MSiW is however consumed by the incorporation of strontium into authigenic carbonates (Solomon et al., 2014); so that the resulting data plots are as observed in Figure 3b. The decreases in both lithium concentrations and Li/Cl ratios in deeper sediments (Figures 2 and 3) can be explained by the incorporation of lithium into newly formed clay minerals during MSiW (Solomon et al., 2014; Wallmann et al., 2008) or during reverse weathering (Stoffyn-Egli & Mackenzie, 1984). Even though the exact mechanism is uncertain, our observations are consistent with lithium consumption by clay minerals at relatively low temperature, as observed elsewhere (Solomon et al., 2014; Stoffyn-Egli & Mackenzie, 1984; Wallmann et al., 2008).

In contrast to the sites with low methane supply, site 920GC displays significant enrichments in lithium and strontium concentrations and high $^{87}Sr/^{86}Sr$ in the deepest three samples (blue area in Figure 3). It is worth noticing that this site is also characterized by high chloride concentration in the fluids (Figure 2), but the increase in lithium is higher than can be attributed uniquely to a brine source (i.e., high Li/Cl ratios in Figure 3). Similar to 940GC and 1522GC, the high $^{87}Sr/^{86}Sr$ ratios can be explained by MSiW, but this reaction cannot explain the elevated lithium content, as no such enrichment was observed at other sites where MSiW is confirmed (Kim et al., 2016; Solomon et al., 2014) nor was it observed in 1522GC and 940GC. Lithium can be released through cation exchange with ammonium under relatively low temperatures (e.g., Chan & Kastner, 2000). The ammonium concentration at 920GC is below 150 μM throughout the core (Hong et al., 2017), a concentration too low to have significant cation exchange with lithium. Additional lithium sources include hydrothermal activity (Stoffyn-Egli & Mackenzie, 1984), opal-A to opal-CT transformation (Gieskes et al.,

1982), interaction with the underlying oceanic and continental crust (Martin et al., 1991; You et al., 1995), and release from clays at high temperature (James et al., 2003). We therefore conclude that the high lithium concentration from 920GC must relate to the water-rock interactions at greater depth (You et al., 1995).

At the sites with shallow SMTZ (911GC, 1520GC, and 1521GC), both lithium content and $^{87}Sr/^{86}Sr$ are close to seawater values (green areas in Figure 3), that is, the pore fluids at these sites present no evidence of MSiW, ion exchange, and/or high temperature water-rock interactions. The lack of any indication of aqueous fluid that originated from the microbial methanogenesis zone and deeper is rather unexpected as active seepages are often associated with a water flux sourced from the deep subsurface (e.g., Haese et al., 2003; Hensen et al., 2004, 2007). We interpret these cation and isotopic signatures to reflect decoupled transport of gaseous and aqueous phases. Multiple lines of evidence indicate that the high methane supply at these sites is sustained by a gaseous phase. Hong et al. (2017) reported the recovery of shallow gas hydrates, which necessitates a gaseous methane source (Bohrmann et al., 1998; Liu & Flemings, 2006; Sultan et al., 2014; Torres et al., 2004). Persistent gas plumes in the water column were observed above these active sites (Serov et al., 2017) at locations where amplitude anomalies indicative of gas accumulation at depth are persistent in the seismic profile (Figure 1c). The stable isotopic signatures from a gas sample taken directly from the bubbles in the water column reveal the thermogenic origin of the gas ($-47.7‰$ and $-242‰$ for $\delta^{13}C\text{-}CH_4$ and $\delta D\text{-}CH_4$, respectively). As this gas pulse moves upward, it saturates the pore space, hinders aqueous advection (Mogollón et al., 2009), and potentially minimizes the diffusion of solutes other than methane, which altogether explains the lack of evidence for chemically altered fluid observed below SMTZ at these active sites.

### 4.2. Different Fluid Transport Modes During the Three Seepage Stages

The contrasting geochemical patterns observed in the six investigated sites not only reflect the complex diagenetic processes and different fluid sources present in this margin but also point to a decoupled transport of water and gas among the different GHMs. Such decoupling between aqueous and gaseous phases has been previously proposed to explain positive pore water chloride anomalies observed at numerous gas hydrate-bearing sites worldwide (Daigle, Bangs, & Dugan, 2011; Daigle & Dugan, 2010; Liu & Flemings, 2006; Peszynska et al., 2016; Torres et al., 2004, 2011). Torres et al. (2004) and Trehu et al. (2004) proposed that the propagation of fractures is enhanced by the excess pore pressure associated with gaseous methane. Liu and Flemings (2006) and Daigle and Dugan (2010) proposed that gaseous methane migrates into the gas hydrate stability zone along a local three-phase equilibrium driven by rapid gas hydrate formation with the resultant high pore water salinity. Despite the different mechanisms proposed, a decoupled migration of gaseous and aqueous phases is well established. Pore space saturated with a gas phase precludes the upward migration of the aqueous phase due to its smaller relative permeability (Lee, 2008). Such interpretation is consistent with the modeling of pore water profiles at 911GC by Hong et al. (2017), who concluded that the advection of aqueous phase is absent at the active sites and diffusion is the main transport mechanism for solutes.

We argue that the observed decoupling of gaseous and aqueous phases in the GHMs reflects the different seepage stages. Based on all our geochemical and geophysical observations, we propose the following three-stage evolution model for Storfjordrenna GHMs (Figure 4). For sites representing the first stage prior to initiation of gas advection ("preactive stage" in Figures 4a and 4b), solute transport is governed by diffusion. During this stage, the pore fluids are influenced by MSiW within the methanogenesis zone, that is, below SMTZ. The release of strontium during MSiW is mostly consumed by authigenic carbonate precipitation while the high $^{87}Sr/^{86}Sr$ signals are preserved and observed from 940GC and 1522GC. Lithium at these sites is incorporated into clay minerals, which results in the concentrations lower than the seawater value. Methane flux is low as the flux is sustained by the inefficient solute diffusion.

The most active stage of the seepage is initiated when the gaseous reservoir is tapped ("active stage" in Figure 4c), possibly driven by hydrofracturing the formation when gas content is high enough to generate the required overpressure (Daigle & Dugan, 2010). Methane is then delivered by the gas advection to the shallow subsurface, which results in the nonsteady state profiles (e.g., 911GC and 1520GC) and promotes the precipitation of shallow gas hydrate (Hong et al., 2017). The gaseous methane discharges at the seafloor in the form of bubble plumes as has been documented by the hydroacoustic surveys (Serov et al., 2017). Gas in the venting bubbles is thermogenic by origin as confirmed by their stable isotopic signatures (Figure 1c). It

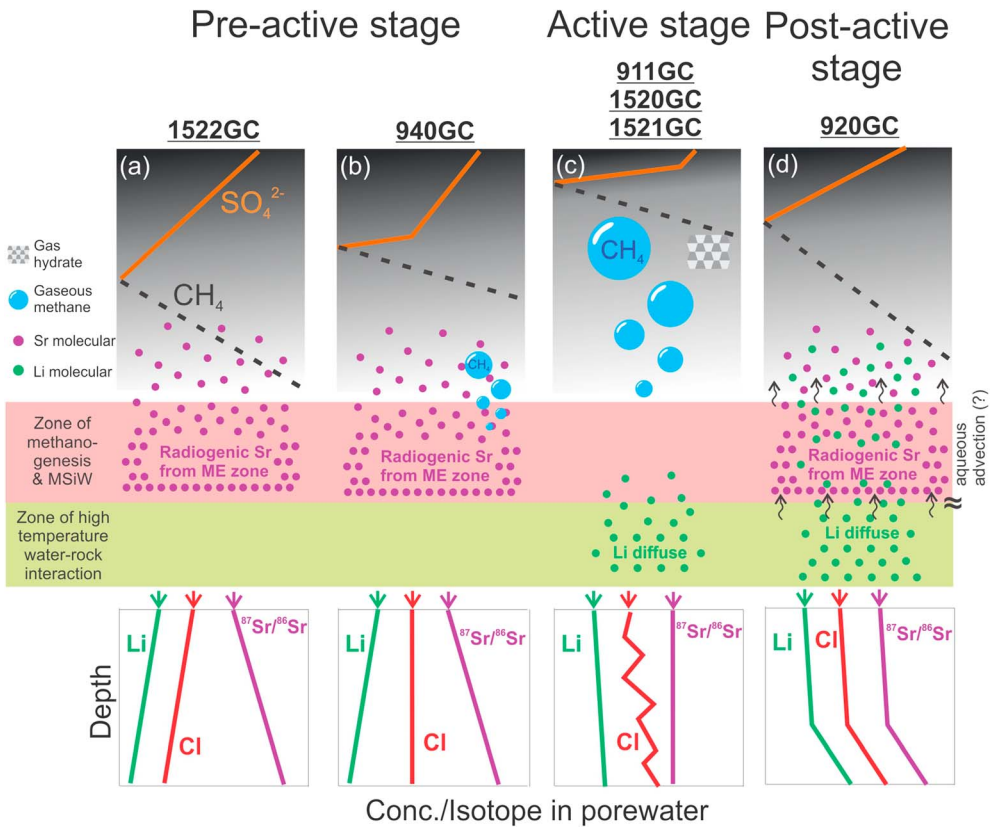


**Figure 4.** We propose that the decoupled transport between gaseous and aqueous phases is related to the different life stages of the investigated gas hydrate mounds. (a) Methane is transported primarily by diffusion during the preactive stage, which explains the smooth sulfate profile observed from 1522GC. (b) At the end of the preactive stage, ascending of gaseous methane induces rapid sulfate consumption through anaerobic oxidation of methane. As the rate is much faster than sulfate diffusion, we observed a nonsteady state sulfate profile from 940GC. (c) During the active stage, the methane supply is sustained by a gaseous phase, which can be mapped by our seismic data in the sediments (Figure 1c). The lack of geochemical proxies for deep aqueous fluid indicates that aqueous advection is mostly absent during this stage. (d) During postactive stage, when the free gas reservoir is exhausted, aqueous advection becomes the primary transport mode carrying methane and other trace elements (e.g., Li) from the greater depth. Contrasting to the sites in the active stage, no gas hydrate was recovered in the first few meters of sediments as dissolved methane is now delivered inefficiently to the shallow subsurface. MSiW = marine silicate weathering.

is likely that the fracture systems underlying the study area provide pathways for deep-sourced gas to migrate upward (Figure 1d), as documented by Mau et al. (2017). During this stage, the transport of gaseous and aqueous phases is decoupled. While methane gas is rapidly ascending, aqueous flow is restricted and solutes in the pore water are only inefficiently transported by diffusion. Such decoupling explains why neither a significant $^{87}Sr/^{86}Sr$ ratio nor changes in lithium concentrations are observed at the active sites.

In response to the exhaustion of a subsurface gaseous reservoir, delivery of gaseous methane terminates ("postactive stage" in Figure 4d). We propose that the draining of the gas reservoir generates low pressures that induces the advection of a deep aqueous phase as inferred from both the high concentration of dissolved lithium and the concave upward shape of the lithium pore water profile at 920GC (Figure 2). The geochemical signal of MSiW (e.g., high $^{87}Sr/^{86}Sr$ ratios) is clearly delivered to the shallow sediments by the ascending aqueous phase. We modified the reduced 1-D model of Hong et al. (2017) and estimated that an advection rate of ~1 cm/year is required to produce the observed lithium profile at this site (see supporting information for more modeling details). Such rate is lower than the advection rates from seep sites with known focused fluid flow such as Hydrate Ridge (50–100 cm/year; Torres et al., 2002), Black Sea (8–25 cm/year; Wallmann et al., 2006), and Bush Hill in the Gulf of Mexico (up to several hundreds of cm/year; Solomon et al.,

2008). We propose that GHM5 reflects the post-active phase of seepage, which contrasts the other four active GHMs in the region (Figure 1b). This inference is supported by the observations that GHM5 is the only mound where no hydroacoustic flares have been detected over the past 3 years of surveys and no gas hydrate was recovered during repeated gravity coring.

It is noted that the availability of gaseous methane and the development of conduits for methane transport largely determine the seepage evolution. Therefore, if a gas supply or a conduit below any of the preactive sites is not in place, the site will never proceed to the next stage. Similarly, if the pore pressure gradient in the sediment column is too small to drive the advection of aqueous phase, diffusion will be the primary process governing the distribution of solutes at the postactive stage. Such dependency on the pressure condition of the underlying fluid flow system is reflected by the spatial heterogeneity of seepage as observed by Hong et al. (2017) and could be explained by our proposed three-state evolution model.

## 5. Conclusions

We compiled observations from pore water geochemistry and geophysical data to document a decoupled fluid transport and evolution of a seepage system in Storfjordrenna, a marine Arctic cold seep. We showed that different fluid transport modes across three life stages (diffusion, gaseous advection, and aqueous advection) characterize the temporal evolution of seepage from the investigated GHMs:

1. A pervasive signal of high $^{87}Sr/^{86}Sr$ ratios in the pore water documents silicate weathering in the microbial methanogenic zone of the sediments. The results of such weathering are neo formation of clay minerals and adsorption of alkali metals such as lithium. Solutes, as well as dissolved methane, are transported primarily by diffusion, which explains the low methane flux and deep SMTZ. This set of condition characterizes the system prior to the initiation of seepage.
2. The initiation of a methane pulse is characterized by rapid advection of gaseous thermogenic methane, which sustains the vigorous bubbling at the seafloor and the formation of massive gas hydrate in the shallow sediments, a similar mechanism as previously proposed (Liu & Flemings, 2006; Torres et al., 2004). Despite the active gas advection, there is no evidence of deep aqueous fluid at this stage as indicated by the seawater-like composition of fluid. These observations can be explained by a decoupled transport of gaseous and aqueous phases, and the barrier of aqueous flow imposed by the low permeability that develops when gas occupies the sediment pore space.
3. After the exhaustion of the gaseous reservoir and the cessation of active gas discharge at the seafloor, a newly generated low pressure induces the advection of the aqueous phase, which results in the high lithium concentration observed from the site representing such postactive stage. Based on the lithium profile, we estimated that the aqueous advection rate is around 1 cm/year at site 920GC from GHM5.

**Acknowledgments**

All geochemical data reported in the paper are included in the Data Set S1 of the supporting information. We would like to acknowledge the captains and crews onboard R/V *Helmer Hanssen* as well as the chief scientists Giuliana Panieri (CAGE15-2) and Jurgen Mienert (CAGE15-6) for the organization and assistance during the cruises. We acknowledge Haoyi Yao for preparing the bathymetry map (Figure 1b) and the sampling work during the cruises. This work was supported by the Research Council of Norway through its Centres of Excellence funding scheme (project 223259), NORCRUST (project 255150), and by the U.S. Department of Energy (DE-FE0013531). We declare no conflict of interest for any coauthors. We also acknowledge Xiaoli Liu and another anonymous reviewer for their constructive comments, which have substantially enhanced the quality of the paper.

## References

Andersen, E. S., Dokken, T. M., Elverhøi, A., Solheim, A., & Fossen, I. (1996). Late Quaternary sedimentation and glacial history of the western Svalbard continental margin. *Marine Geology*, *133*(3-4), 123–156. https://doi.org/10.1016/0025-3227(96)00022-9

Boetius, A., & Wenzhofer, F. (2013). Seafloor oxygen consumption fuelled by methane from cold seeps. *Nature Geoscience*, *6*(9), 725–734. https://doi.org/10.1038/ngeo1926

Bohrmann, G., Greinert, J., Suess, E., & Torres, M. (1998). Authigenic carbonates from the Cascadia subduction zone and their relation to gas hydrate stability. *Geology*, *26*(7), 647–650. https://doi.org/10.1130/0091-7613(1998)026%3C0647:ACFTCS%3E2.3.CO;2

Breivik, A. J., Mjelde, R., Grogan, P., Shimamura, H., Murai, Y., & Nishimura, Y. (2003). Crustal structure and transform margin development south of Svalbard based on ocean bottom seismometer data. *Tectonophysics*, *369*(1-2), 37–70. https://doi.org/10.1016/S0040-1951(03)00131-8

Chan, L.-H., & Kastner, M. (2000). Lithium isotopic compositions of pore fluids and sediments in the Costa Rica subduction zone: Implications for fluid processes and sediment contribution to the arc volcanoes. *Earth and Planetary Science Letters*, *183*(1-2), 275–290. https://doi.org/10.1016/S0012-821X(00)00275-2

Chen, N. C., Yang, T. F., Hong, W. L., Chen, H. W., Chen, H. C., Hu, C. Y., et al. (2017). Production, consumption, and migration of methane in accretionary prism of southwestern Taiwan. *Geochemistry, Geophysics, Geosystems*, *18*, 2970–2989. https://doi.org/10.1002/2017GC006798

Daigle, H., Bangs, N. L., & Dugan, B. (2011). Transient hydraulic fracturing and gas release in methane hydrate settings: A case study from southern Hydrate Ridge. *Geochemistry, Geophysics, Geosystems*, *12*, Q12022. https://doi.org/10.1029/2011GC003841

Daigle, H., & Dugan, B. (2010). Effects of multiphase methane supply on hydrate accumulation and fracture generation. *Geophysical Research Letters*, *37*, L20301. https://doi.org/10.1029/2010GL044970

Elverhøi, A., & Solheim, A. (1983). The Barents Sea ice sheet—A sedimentological discussion. *Polar Research*, *1*(1), 23–42. https://doi.org/10.3402/polar.v1i1.6968

Engen, Ø., Faleide, J. I., & Dyreng, T. K. (2008). Opening of the Fram Strait gateway: A review of plate tectonic constraints. *Tectonophysics*, *450*(1-4), 51–69. https://doi.org/10.1016/j.tecto.2008.01.002

Gabrielsen, R. (1984). Long-lived fault zones and their influence on the tectonic development of the southwestern Barents Sea. *Journal of the Geological Society*, *141*(4), 651–662. https://doi.org/10.1144/gsjgs.141.4.0651

Gieskes, J. M., Elderfield, H., Lawrence, J. R., Johnson, J., Meyers, B., & Campbell, A. (1982). 16. Geochemistry of interstitial waters and sediments, leg 64, Gulf of California1. Initial Reports of the Deep Sea Drilling Project: A Project Planned by and Carried Out with the Advice of the Joint Oceanographic Institutions for Deep Earth Sampling 64: 675.

Greinert, J., Lewis, K., Bialas, J., Pecher, I. A., Rowden, A., Bowden, D., et al. (2010). Methane seepage along the Hikurangi margin, New Zealand: Overview of studies in 2006 and 2007 and new evidence from visual, bathymetric and hydroacoustic investigations. *Marine Geology*, *272*(1-4), 6–25. https://doi.org/10.1016/j.margeo.2010.01.017

Greinert, J., Veloso, M., De Batist, M. A., & Mienert, J. (2013). Hydroacoustic quantification of free-gas venting offshore Svalbard, Arctic: Changes in space and time. AGU Fall Meeting Abstracts.

Haeckel, M., Suess, E., Wallmann, K., & Rickert, D. (2004). Rising methane gas bubbles form massive hydrate layers at the seafloor. *Geochimica et Cosmochimica Acta*, *68*(21), 4335–4345. https://doi.org/10.1016/j.gca.2004.01.018

Haese, R. R., Meile, C., Van Cappellen, P., & De Lange, G. J. (2003). Carbon geochemistry of cold seeps: Methane fluxes and transformation in sediments from Kazan mud volcano, eastern Mediterranean Sea. *Earth and Planetary Science Letters*, *212*(3–4), 361–375. https://doi.org/10.1016/S0012-821X(03)00226-7

Haydon, P. R., & Graf, D. L. (1986). Studies of smectite membrane behavior: Temperature dependence, 20–180°C. *Geochimica et Cosmochimica Acta*, *50*(1), 115–121. https://doi.org/10.1016/0016-7037(86)90055-4

Hensen, C., Wallmann, K., Schmidt, M., Liebetrau, V., Fehn, U., Garbe-Schonberg, D., & Bruckmann, W. (2007). Geochemistry of cold vent fluids at the central American convergent margin. *Geochimica et Cosmochimica Acta*, *71*(15), A396–A396.

Hensen, C., Wallmann, K., Schmidt, M., Ranero, C. R., & Suess, E. (2004). Fluid expulsion related to mud extrusion off Costa Rica—A window to the subducting slab. *Geology*, *32*(3), 201–204. https://doi.org/10.1130/G20119.1

Hong, W. L., Torres, M. E., Carroll, J., Cremiere, A., Panieri, G., Yao, H., & Serov, P. (2017). Seepage from an Arctic shallow marine gas hydrate reservoir is insensitive to momentary ocean warming. *Nature Communications*. https://doi.org/10.1038/ncomms15745

Hovland, M., Judd, A. G., & Burke, R. A. (1993). The global flux of methane from shallow submarine sediments. *Chemosphere*, *26*(1-4), 559–578. https://doi.org/10.1016/0045-6535(93)90442-8

Ingólfsson, Ó., & Landvik, J. Y. (2013). The Svalbard–Barents Sea ice-sheet—Historical, current and future perspectives. *Quaternary Science Reviews*, *64*, 33–60. https://doi.org/10.1016/j.quascirev.2012.11.034

James, R. H., Allen, D. E., & Seyfried, W. E. (2003). An experimental study of alteration of oceanic crust and terrigenous sediments at moderate temperatures (51 to 350°C): Insights as to chemical processes in near-shore ridge-flank hydrothermal systems. *Geochimica et Cosmochimica Acta*, *67*(4), 681–691. https://doi.org/10.1016/S0016-7037(02)01113-4

Kastner, M., Elderfield, H., & Martin, J. B. (1991). Fluids in convergent margins: What do we know about their composition, origin, role in diagenesis and importance for oceanic chemical fluxes? *Philosophical Transactions: Physical Sciences and Engineering*, *335*(1638), 243–259. https://doi.org/10.1098/rsta.1991.0045

Kim, J. H., Torres, M. E., Haley, B. A., Ryu, J. S., Park, M. H., Hong, W. L., & Choi, J. (2016). Marine silicate weathering in the anoxic sediment of the Ulleung Basin: Evidence and consequences. *Geochemistry, Geophysics, Geosystems*, *17*, 3437–3453. https://doi.org/10.1002/2016GC006356

Kim, J.-H., Torres, M. E., Hong, W.-L., Choi, J., Riedel, M., Bahk, J. J., & Kim, S.-H. (2013). Pore fluid chemistry from the second gas hydrate drilling expedition in the Ulleung Basin (UBGH2): Source, mechanisms and consequences of fluid freshening in the central part of the Ulleung Basin, East Sea. *Marine and Petroleum Geology*, *47*, 99–112. https://doi.org/10.1016/j.marpetgeo.2012.12.011

Kvenvolden, K. A., & Rogers, B. W. (2005). Gaia's breath—Global methane exhalations. *Marine and Petroleum Geology*, *22*(4), 579–590. https://doi.org/10.1016/j.marpetgeo.2004.08.004

Lee, M. W. (2008). Models for gas hydrate-bearing sediments inferred from hydraulic permeability and elastic velocities. Scientific Investigations Report 2008–5219, U.S. Department of the Interior, U.S. Geological Survey (pp. 14).

Liu, X. L., & Flemings, P. B. (2006). Passing gas through the hydrate stability zone at southern hydrate ridge, offshore Oregon. *Earth and Planetary Science Letters*, *241*(1–2), 211–226. https://doi.org/10.1016/j.epsl.2005.10.026

MacDonald, I., Guinasso, N., Sassen, R., Brooks, J., Lee, L., & Scott, K. (1994). Gas hydrate that breaches the sea floor on the continental slope of the Gulf of Mexico. *Geology*, *22*(8), 699–702. https://doi.org/10.1130/0091-7613(1994)022%3C0699:GHTBTS%3E2.3.CO;2

Martin, J. B., Kastner, M., & Elderfield, H. (1991). Lithium: Sources in pore fluids of Peru slope sediments and implications for oceanic fluxes. *Marine Geology*, *102*(1-4), 281–292. https://doi.org/10.1016/0025-3227(91)90012-S

Mau, S., Römer, M., Torres, M., Bussmann, I., Pape, T., Damm, E., et al. (2017). Widespread methane seepage along the continental margin off Svalbard-from Bjørnøya to Kongsfjorden. *Scientific Reports*, *7*. https://doi.org/10.1038/srep42997

McVeigh, D., Skarke, A., Dekas, A. E., Borrelli, C., Hong, W. L., Marlow, J. J., et al. (2018). Characterization of benthic biogeochemistry and ecology at three methane seep sites on the northern U.S. Atlantic margin. *Deep Sea Research Part II: Topical Studies in Oceanography*. https://doi.org/10.1016/j.dsr2.2018.03.001

Mogollón, J. M., L'Heureux, I., Dale, A. W., & Regnier, P. (2009). Methane gas-phase dynamics in marine sediments: A model study. *American Journal of Science*, *309*(3), 189–220. https://doi.org/10.2475/03.2009.01

Mörner, N.-A. (1978). Faulting, fracturing, and seismicity as functions of glacio-isostasy in Fennoscandia. *Geology*, *6*(1), 41–45. https://doi.org/10.1130/0091-7613(1978)6%3C41:FFASAF%3E2.0.CO;2

Myhre, A. M., Eldholm, O., & Sundvor, E. (1982). The margin between Senja and Spitsbergen fracture zones: Implications from plate tectonics. *Tectonophysics*, *89*(1–3), 33–50. https://doi.org/10.1016/0040-1951(82)90033-6

Nikolovska, A., Sahling, H., & Bohrmann, G. (2008). Hydroacoustic methodology for detection, localization, and quantification of gas bubbles rising from the seafloor at gas seeps from the eastern Black Sea. *Geochemistry, Geophysics, Geosystems*, *9*, Q10010. https://doi.org/10.1029/2008GC002118

Patton, H., Hubbard, A., Andreassen, K., Winsborrow, M., & Stroeven, A. P. (2016). The build-up, configuration, and dynamical sensitivity of the Eurasian ice-sheet complex to late Weichselian climatic and oceanic forcing. *Quaternary Science Reviews*, *153*, 97–121. https://doi.org/10.1016/j.quascirev.2016.10.009

Peszynska, M., Hong, W.-L., Torres, M. E., & Kim, J.-H. (2016). Methane hydrate formation in Ulleung Basin under conditions of variable salinity: Reduced model and experiments. *Transport in Porous Media*, *114*(1), 1–27. https://doi.org/10.1007/s11242-016-0706-y

Petersen, C. J., Bünz, S., Hustoft, S., Mienert, J., & Klaeschen, D. (2010). High-resolution P-cable 3D seismic imaging of gas chimney structures in gas hydrated sediments of an Arctic sediment drift. *Marine and Petroleum Geology*, *27*(9), 1981–1994. https://doi.org/10.1016/j.marpetgeo.2010.06.006

Post, V. E., Groen, J., Kooi, H., Person, M., Ge, S., & Edmunds, W. M. (2013). Offshore fresh groundwater reserves as a global phenomenon. *Nature*, *504*(7478), 71–78. https://doi.org/10.1038/nature12858

Rasmussen, T., & Thomsen, E. (2014). Brine formation in relation to climate changes and ice retreat during the last 15,000 years in Storfjorden, Svalbard, 76–78°N. *Paleoceanography*, *29*, 911–929. https://doi.org/10.1002/2014PA002643

Reeburgh, W. S. (2007). Oceanic methane biogeochemistry. *Chemical Reviews*, *107*(2), 486–513. https://doi.org/10.1021/cr050362v

Regnier, P., Dale, A. W., Arndt, S., LaRowe, D. E., Mogollon, J., & Van Cappellen, P. (2011). Quantitative analysis of anaerobic oxidation of methane (AOM) in marine sediments: A modeling perspective. *Earth-Science Reviews*, *106*(1–2), 105–130. https://doi.org/10.1016/j.earscirev.2011.01.002

Römer, M., Sahling, H., Pape, T., Bahr, A., Feseker, T., Wintersteller, P., & Bohrmann, G. (2012). Geological control and magnitude of methane ebullition from a high-flux seep area in the Black Sea—The Kerch seep area. *Marine Geology*, *319–322*, 57–74.

Sahling, H., Römer, M., Pape, T., Bergès, B., dos Santos Fereirra, C., Boelmann, J., et al. (2014). Gas emissions at the continental margin west off Svalbard: Mapping, sampling, and quantification. *Biogeosciences Discussions*, *11*(5), 7189–7234. https://doi.org/10.5194/bgd-11-7189-2014

Sauter, E. J., Muyakshin, S. I., Charlou, J. L., Schluter, M., Boetius, A., Jerosch, K., et al. (2006). Methane discharge from a deep-sea submarine mud volcano into the upper water column by gas hydrate-coated methane bubbles. *Earth and Planetary Science Letters*, *243*(3–4), 354–365. https://doi.org/10.1016/j.epsl.2006.01.041

Serov, P., Vadakkepuliyambatta, S., Mienert, J., Patton, H., Portnov, A., Silyakova, A., et al. (2017). Postglacial response of Arctic Ocean gas hydrates to climatic amelioration. *Proceedings of the National Academy of Sciences of the United States of America*, *114*(24), 6215–6220. https://doi.org/10.1073/pnas.1619288114

Skogseth, R., Haugan, P. M., & Jakobsson, M. (2005). Watermass transformations in Storfjorden. *Continental Shelf Research*, *25*(5–6), 667–695. https://doi.org/10.1016/j.csr.2004.10.005

Smith, A. J., Mienert, J., Bunz, S., & Greinert, J. (2014). Thermogenic methane injection via bubble transport into the upper Arctic Ocean from the hydrate-charged Vestnesa Ridge, Svalbard. *Geochemistry, Geophysics, Geosystems*, *15*, 1945–1959. https://doi.org/10.1002/2013GC005179

Solomon, E. A., Kastner, M., Jannasch, H., Robertson, G., & Weinstein, Y. (2008). Dynamic fluid flow and chemical fluxes associated with a seafloor gas hydrate deposit on the northern Gulf of Mexico slope. *Earth and Planetary Science Letters*, *270*(1-2), 95–105. https://doi.org/10.1016/j.epsl.2008.03.024

Solomon, E. A., Spivack, A. J., Kastner, M., Torres, M. E., & Robertson, G. (2014). Gas hydrate distribution and carbon sequestration through coupled microbial methanogenesis and silicate weathering in the Krishna–Godavari Basin, offshore India. *Marine and Petroleum Geology*, *58*(Part A), 233–253. https://doi.org/10.1016/j.marpetgeo.2014.08.020

Stewart, I. S., Sauber, J., & Rose, J. (2000). Glacio-seismotectonics: Ice sheets, crustal deformation and seismicity. *Quaternary Science Reviews*, *19*(14–15), 1367–1389. https://doi.org/10.1016/S0277-3791(00)00094-9

Stoffyn-Egli, P., & Mackenzie, F. T. (1984). Mass balance of dissolved lithium in the oceans. *Geochimica et Cosmochimica Acta*, *48*(4), 859–872. https://doi.org/10.1016/0016-7037(84)90107-8

Sultan, N., Bohrmann, G., Ruffine, L., Pape, T., Riboulot, V., Colliat, J. L., et al. (2014). Pockmark formation and evolution in deep water Nigeria: Rapid hydrate growth versus slow hydrate dissolution. *Journal of Geophysical Research: Solid Earth*, *119*, 2679–2694. https://doi.org/10.1002/2013JB010546

Sundvor, E., & Eldholm, O. (1976). *Marine geophysical survey on the continental margin from Bear Island to Hornsund*. Spitsbergen: Observatory, University.

Torres, M. E., Kim, J.-H., Choi, J.-Y., Ryu, B.-J., Bahk, J.-J., Riedel, M., et al. (2011). Occurrence of high salinity fluids associated with massive near-seafloor gas hydrate deposits. 7th International Conference on Gas Hydrates. Edinburgh, Scotland, United Kingdom.

Torres, M. E., McManus, J., Hammond, D. E., de Angelis, M. A., Heeschen, K. U., Colbert, S. L., et al. (2002). Fluid and chemical fluxes in and out of sediments hosting methane hydrate deposits on hydrate ridge, OR, I: Hydrological provinces. *Earth and Planetary Science Letters*, *201*(3–4), 525–540. https://doi.org/10.1016/S0012-821X(02)00733-1

Torres, M. E., Wallmann, K., Trehu, A. M., Bohrmann, G., Borowski, W. S., & Tomaru, H. (2004). Gas hydrate growth, methane transport, and chloride enrichment at the southern summit of Hydrate Ridge, Cascadia margin off Oregon. *Earth and Planetary Science Letters*, *226*(1–2), 225–241. https://doi.org/10.1016/j.epsl.2004.07.029

Trehu, A. M., Flemings, P. B., Bangs, N. L., Chevallier, J., Gracia, E., Johnson, J. E., et al. (2004). Feeding methane vents and gas hydrate deposits at south Hydrate Ridge. *Geophysical Research Letters*, *31*, L23310. https://doi.org/10.1029/2004GL021286

Ussler, W., & Paull, C. K. (2001). Ion exclusion associated with marine gas hydrate deposits. *Natural gas hydrates: Occurrence, distribution, and detection* (pp. 41–51). Washington, DC: American Geophysical Union.

Wallmann, K., Aloisi, G., Haeckel, M., Tishchenko, P., Pavlova, G., Greinert, J., et al. (2008). Silicate weathering in anoxic marine sediments. *Geochimica et Cosmochimica Acta*, *72*(12), 2895–2918. https://doi.org/10.1016/j.gca.2008.03.026

Wallmann, K., Drews, M., Aloisi, G., & Bohrmann, G. (2006). Methane discharge into the Black Sea and the global ocean via fluid flow through submarine mud volcanoes. *Earth and Planetary Science Letters*, *248*(1–2), 545–560. https://doi.org/10.1016/j.epsl.2006.06.026

Wallmann, K., Riedel, M., Hong, W. L., Patton, H., Hubbard, A., Pape, T., et al. (2018). Gas hydrate dissociation off Svalbard induced by isostatic rebound rather than global warming. *Nature communications*, *9*(1), 83. https://doi.org/10.1038/s41467-017-02550-9

Wegner, C., Bennett, K. E., de Vernal, A., Forwick, M., Fritz, M., Heikkilä, M., et al. (2015). Variability in transport of terrigenous material on the shelves and the deep Arctic Ocean during the Holocene. *Polar Research*, *34*(1), 24964. https://doi.org/10.3402/polar.v34.24964

You, C.-F., Chan, L., Spivack, A., & Gieskes, J. (1995). Lithium, boron, and their isotopes in sediments and pore waters of Ocean Drilling Program site 808, Nankai trough: Implications for fluid expulsion in accretionary prisms. *Geology*, *23*(1), 37–40. https://doi.org/10.1130/0091-7613(1995)023%3C0037:LBATII%3E2.3.CO;2